

First lamina hybridization of high performance CFRP with Kevlar fibers: Effect on impact behavior and nondestructive evaluation

Carmelo Militello^a, Gabriella Epasto^{b*}, Francesco Bongiorno^a, Bernardo Zuccarello^a

^a *Università degli Studi di Palermo - Dipartimento di Ingegneria, Viale delle Scienze, 90128 Palermo (Italy)*

^b *Università degli Studi di Messina - Dipartimento di Ingegneria, Contrada di Dio, Villaggio Sant'Agata 98166 Messina (Italy)*

E-mail address of the authors:

Carmelo Militello, *carmelo.militello01@unipa.it*

Gabriella Epasto, *gabriella.epasto@unime.it*

Francesco Bongiorno, *francesco.bongiorno01@unipa.it*

Bernardo Zuccarello, *bernardo.zuccarello@unipa.it*

*Corresponding author

Gabriella Epasto

University of Messina

Contrada di Dio, Villaggio Sant'Agata 98166 Messina, Italy

e-mail: *gabriella.epasto@unime.it*

Number of words: 8081

Lamina hybridization in high performance CFRP: effect on impact behavior and non-destructive evaluation

Abstract

The impact behavior of carbon-aramid hybrid composites was evaluated. To highlight the hybridization effect, comparative analyses were performed with the basic CFRP laminate having the same lay-up. Tensile and low velocity impact tests, followed by non-destructive inspections, highlighted that the hybrid composite showed an increment in specific impact strength up to 50%, with a relevant increase in the maximum specific impact force. To assess the most reliable technique to detect the impact damage, non-destructive evaluation was performed by pulsed thermography, phased array ultrasonic technique, computed tomography and digital radiography. Phased array ultrasonic technique can be considered the most appropriate technique.

Keywords: Hybrid composites, low velocity impact, damage assessment, phased array ultrasonic technique; x-rays techniques; infrared thermography.

1. Introduction

Polymer-matrix composites (PMCs) have assumed an indispensable role in the automotive industry, due to their main characteristics of high specific strength and stiffness compared to traditional materials. It has been estimated that the use of polymer composites reinforced with glass or carbon fibers for the manufacturing of structural components, reduces the weight of the vehicle by 35 and 60%, respectively [1].

However, in order to better tailor the use of these materials in the various specific applications, as well as to improve furtherly the automotive performance, the design of these materials requires increasingly high performance targets, and the so-called hybridization technique consisting in general into the combination of two or more types of fibers.

Although recently the hybridization of reinforcements of different kinds in PMCs has been also used to improve the environmental sustainability, by adding natural fiber to synthetic fibers [2-8], or to optimize (reduce) the cost of the material by introducing carbon nanofiber electrospun that can replace conventional CFRP [9], or again to ensure carbon fibers to improve GFRP along the main loading path [10]; the improvement of the mechanical performance of composite materials for extreme applications, especially in competitions, continues to be one of the key drivers of research into so-called hybrid innovative materials. In the literature there are several works [11-21] where the hybridization technique, used for the development of high performance composites reinforced with synthetic fibers, leads to significant increases in static mechanical properties. In [12,13], Batista et al. have analysed the presence of geometric discontinuities and the influence of environmental aging on the mechanical properties of carbon/kevlar and carbon/glass hybrid composites. The authors have demonstrated that not only the resin type plays a crucial role in the structural integrity of the analyzed composite, but also the fiber type, since the fiber/matrix interface depends on their combination.

From the point of view of dynamic mechanical properties, hybridisation has been applied in [22-25] to obtain increases in impact resistance of carbon fibre reinforced composites by introducing ductile fibres such as kevlar and glass fibres, respectively.

In literature, many authors faced the challenge to evaluate the impact damage in composite materials through the application of non-destructive techniques. Caminero et al. [26] and Papa et al. [27] used phased array ultrasonic technique to identify damage in CFRP, 3D printed reinforced composites [26] and hybrid laminates, reinforced with carbon and glass woven layers [27], respectively. Moradi et Safizadeh [28] proposed

step heating thermography method to investigate debondings in carbon/epoxy patches. Meola et al. [29] used both phased array ultrasonic technique and infrared thermography to evaluate damage in CFRP during impact event. Rubio Díaz et al. [30] analyzed failure mechanisms in aramid composites for ballistic applications by computed tomography e profilometry. Guo et al. [31] analyzed the effect of hybridization of carbon/glass fiber reinforced composite rods by digital image correlation technique. Gaudenzi et al. [32] and Epasto et al. [33,34] analysed the performances of ultrasonic and infrared techniques for the inspection of composite laminates subjected to impact damage.

Unlike all these research papers on this topic, the present study focuses on an extensive non-destructive evaluation (NDE) of impact damage in high performance hybrid C-KFRP, by considering not only the hybridization effect on mechanical properties but also the application of different advanced non-destructive techniques (NDT).

In this experimental study, the effect of hybridisation in composites on static and impact mechanical properties has been evaluated. In more detail, a hybrid cross-ply fabric, made of carbon fibre and kevlar, has been introduced on the surface of a CFRP laminates used to the manufacturing of mechanical component which are mainly subject to impact loading. Tensile test, 3-point bending test and impact tests have been carried out in order to assess the effect of hybridisation in such highly performing composites used for applications characterized by possible impact events (ailerons (Figure 1a), bumpers (Figure 1b), etc.).

[Figure 1 near here]

Extensive NDE has been carried out with advanced techniques: pulsed thermography (PT), phased array ultrasonic technique (PAUT), computed tomography (CT) and digital radiography (DR), in order to assess the most reliable, easy-to-apply, and time-saving technique for quantifying the impact damage. Considering that the impact event can happen during the operating phase of the components, particular attention was put in the on-site applicability of the proposed techniques, as well as the capability to resolve the different damage mechanisms. This last aspect was considered in order to compare the different techniques and to find a relationship between the impact energy and the mechanical damage.

2. Materials and methods

2.1 *Laminate composite manufacturing*

The considered hybrid C-KFRP composite material is widely used for sport automotive applications. It is generally manufactured by hand lay-up with subsequent vacuum bag and autoclave curing processes with $T_{\max}=125\text{ }^{\circ}\text{C}$ and $P_{\max}=5\text{ bar}$ for about two hours, by using pre-pregs laminae supplied by Delta-Preg S.p.a., in accordance with a defined stacking sequences reported in **Errore. L'origine riferimento non è stata trovata..** In more detail, this C-KRFP is constituted by a surface lamina reinforced by a twill type hybrid fabric (GA210T, specific weight of 210 g/m^2) consisting of alternating yarns in carbon and kevlar fibers, superimposed to two laminae reinforced by twill type carbon fabrics (C630T, specific weight of 630 g/m^2). The homogeneous basic CFRP laminate, properly analyzed to highlight the hybridization effects, is constituted by three laminae reinforced by the same twill type carbon fabric C630T, with the lay-up reported in **Errore. L'origine riferimento non è stata trovata..**

[Table 1 near here]

An optimized cure process has been applied to both laminates (by respecting appropriate pressure and temperature cycles) to obtain a finished material with a very low percentage of micro voids, ensuring the best mechanical properties. Both laminates panels so obtained (having dimension of 250x250 mm) have been cut by using a circular saw in order to achieve the different specimens necessary to performs the tensile, 3-point bending and low-velocity impact tests, in accordance to the relative standard.

2.2 Mechanical testing

Static tensile and three-point bending tests were carried out by using of a servo-hydraulic testing machine type MTS 810, instrumented by an MTS extensometer having a gauge length of 25 mm.

In accordance with ASTM D3039 standard [35], the tensile tests have been performed in displacement control with a speed of 1 mm/min; five rectangular specimens, measuring 25x250 mm, have been tested for each sample (see Figure 13a).

[Figure 2 near here]

The same displacement control procedure has been used for the three-point bending tests, but with a speed of 2 mm/min. Specimens sizes have been produced in accordance with ASTM D7264 [36]: width equal to 12.5 mm and fixed length in accordance with support-span/thickness ratio of 16, increased by 20% (see Figure 13b). Five test specimens for each type of composite analyzed in this work, were tested by three-point bending.

The analyzed composite laminates have been also tested at low-velocity impact by performing drop tests in accordance with ISO 6603-2 standard [37]. The impact tests have been carried out by using the *Ceast Fractovis Plus* test machine instrumented by an anti-rebound system that does not allow the occurrence of multiple impacts. The impactor has a hemispherical tip with a nominal diameter of 20 mm. During the impact test, the impactor transfers the kinetic energy of the drop mass through the impact contact to the test specimen of size 60x60 mm, the specimens have been simply supported on a rigid metallic ring having an internal diameter of 40 mm (see Figure 13c). Impact tests have been carried out at impact energy levels E_i varying from 20 to 35 J with steps of 5 J, by using 3 specimens per each energy level. Additional impact tests at 10 and 15 J were performed for the hybrid specimens, in order to obtain a complete characterization of damage also at low loads. The results of such tests are reported in the following section devoted to the non-destructive damage evaluation and have been useful to build the impact energy vs. impact damage charts. In accordance with the final application of these composite laminates, both types of material considered have been exposed to the impact in the face formed by the first 0/90 lamina. During the impact test, the test machine allows the acquisition (with frequency of 2 MHz) of the impact force F_i transferred from the impactor to the test specimen, as well as of the displacement s of the impactor and the impact velocity v_i .

2.3 Non-destructive damage evaluation

Non-destructive evaluation of the damage due to impact has been performed by using X-ray computed tomography (CT) with a 250 μm focal spot size; voltage and current were set to 190 kV and 1 mA, respectively. A Cu beam filter having a thickness of 1 mm was put between the tube and the specimen. For the reconstruction, a voxel resolution of 45 $\mu\text{m} \times 45 \mu\text{m} \times 45 \mu\text{m}$ was chosen, with a pixel resolution in tomogram

of 2048×2048 . The dataset was processed by VGStudio Max 2.0 (Volume Graphics GmbH, Heidelberg, Germany) and the rendering tools used for 3D reconstructions were sum along X-rays and maximum projection. CT allowed to analyze in detail the extension and the type of damage of the C-KFRP specimens, under low-velocity impact loading. The tomograms corresponding to the maximum indentation, due to the impact, were analyzed as well.

The tested CFRP specimens were subjected to digital radiographic inspection (DR). The radiographic evaluation was performed with a Bosello SRE m@x system. The radiographic machine is equipped with X-ray tube having a maximum voltage of 320 kV and a focal spot size of 400 μm . The detector is a flat panel with a resolution of 1024×1024 pixels. The system is equipped with a manipulator having an automatic 4-axes movement control system. The radiographic images were obtained by setting the X-ray source at a voltage of 45 kV and a current of 0.6 mA. Radiographies were processed with inbuilt Imaging Processing software from Bosello High Technology (IP BHT Plus image processor), and a median EN filter was applied to improve the signal-to-noise ratio in the radiographic images.

Phased array ultrasonic technique (PAUT) inspection was used to analyze the damage of both the analyzed composites. In detail, PAUT was performed by using Olympus Focus PX 16/128 acquisition unit with FocusPC software and a 64 elements linear near-wall probe at 3.5 MHz (3.5 L64-NW1, 64 mm aperture, 1 mm pitch, 7 mm elevation) equipped with a wedge SNW1-0 L-IHC and with a Versa MOUSE encoder. Longitudinal waves velocity was calculated, which was equal to 2769 m/s for the CFRP and 2615 m/s for the C-KFRP. The impact damage was analyzed by using both S-scan and C-scan.

Pulsed (flash) Thermography (PT) analyses were carried using a Flir Systems X8400sc thermal camera having thermal sensitivity of 20 mK @ 30°C, with a sub-windowing of 640×512 pixels. The Infrared (IR) thermal camera is equipped with Focal Plane Array (FPA) cooled InSb detector. The frame rate was set to 150 fps. The thermograms were post-processed with Flir ResearcherIR Max software by using image subtraction operations. The thermal camera was placed on a tripod at a distance of 0.25 m from the sample; the instant field of view (IFOV = 67 microrad) was calculated for the mounted IR lens, having focal length 24 mm. The flash was placed near the camera.

All the techniques allowed the measurements of maximum damage size (d_{max}) for the investigated specimens subjected to impact tests.

3. Results and discussion

3.1 *Static mechanical properties*

3.1.1 *Tensile test*

In Figure 14, the tensile curves of both the analyzed composite laminates, are depicted in detail.

[Figure 3 near here]

From the Figure 14 it is seen how the substitution of the surface carbon lamina with the carbon-kevlar lamina leads to an appreciable reduction of the tensile strength (about -30%): approximately equal to 700 MPa and 480 MPa for the carbon-fibre reinforced composite and the hybrid composite, respectively. As expected also in terms of stiffness, the hybridization leads to a reduction of the Young's Modulus, from about 39 GPa for the CFRP laminate to about 33 GPa for the hybrid C-KFRP laminate (about

-15%). As expected too, the hybrid laminate exhibits a progressive damaging associated to the different mechanical behavior of carbon and aramid fibers, with a consequent nonlinear trend of the second part of tensile curve. This progressive damage (aramid fibers fail after carbon fibers) explains also the reduction of the tensile strength. In the basic CFRP laminate, in fact, the damage is concentrated at the failure load which is reacted with a linear elastic behavior (brittle failure).

3.1.2 *Tree-point bending test*

Three-point bending tests have been carried out on the analyzed composites in order to assess also the influence of the hybridization on the bending strength of the CFRP laminate. Figure 15 shows the bending curves relative to the two laminates, considering the two different load conditions corresponding to the load applied into the (0/90) first lamina and the load applied to the ultimate (± 45) lamina. Such two different bending configurations have been considered in order to examine in detail the expected different behavior of the non-symmetrical laminates considered (actually, used in car manufacturing).

[Figure 4 near here]

In more detail, Figure 15a shows how the basic CFRP laminate exhibits better performance when, as expected, 0° fibers are subjected to tensile load, with a bending strength increment respect to the opposite configuration of about +15% (from about 480 MPa to about 550 MPa); in other words, although this configuration with the lamina (0/90) subject to the extensive compressive loading is that used in practice by the car manufactures for component subjected to impact loading, it is that which leads to the lower static bending strength. Similar results are obtained from Figure 15b for the

hybrid laminate: the configuration with hybrid lamina subjected to the tensile load leads to the higher strength (the 0° carbon fiber are subjected to tensile load) whereas the actual service configuration selected by the manufactured in which the hybrid lamina is subjected to the compressive load leads to the lower strength (appreciable reduction of about -18%) but at the same time to more progressive damage mechanism with higher failure strain and, most important, higher failure energy. Taking into account that to improve the impact strength it is necessary to reduce the maximum force and to increase the maximum failure strain and consequently the maximum energy to failure, such result corroborate that hybridization of the surface lamina (0/90) is the best way to obtain impact strength improvements.

The following Table 1 shows synthetically the bending mechanical properties of the analyzed laminates.

[Table 2 near here]

From Table 1 it is seen how the two laminates exhibits similar bending modulus of about 21/23 GPa, i.e. the hybridization do not lead to significant stiffness variations. Also, the bending strength values are very close for the different laminates depending mainly on the test configuration, i.e. on the sign of the stress acting on the 0° carbon fibers. It passes from about 480 MPa to about 560 MPa switching from one configuration to another.

The failure energy instead increases considerable by hybridization, specially by considering the actual service configuration with 0/90 hybrid lamina at the loaded surface.

3.2 *Impact properties*

For each material and for each impact energy level, Figure 1 shows the corresponding plots of the impact load-time curve $F_i(t)$ and of the impact load-displacement curve $F_i(s)$.

[Figure 5 near here]

Such curves allow an immediate detection of the main characteristic parameters that define the behavior of the material under low-velocity impact loading, such as the actual duration of the impact phenomenon as well as the peak force or maximum impact force F_i^{MAX} that can be detected from both the curves. In particular, the curve $F_i(s)$ allows to evaluate the energy E_a absorbed by the specimen, corresponding to the closed integral of the curve; it is constituted in practice by the energy $E_{a,e}$ (area underlying to the linear segment of the curve) absorbed during the elastic phase, and the energy $E_{a,p}$ (area underlying to the successive non-linear segment of the curve) dissipated through elasto-plastic damaging processes of the specimen. In addition, in the absence of full penetration the curves $F_i(s)$ (see again Figure 1b and 5d), permit also to detect the so called elastic return energy expressed by the area underlying the curve segment that represents the contemporary monotonous reduction of both displacement and load. Obviously, it is in practice the energy returned to the impactor, given by the difference of the impacting energy and the energy absorbed by the specimen.

According to the experimental evidence, such impact curves reported in Figure 1, allow to observe the complete penetration of the hybrid C-KFRP laminate that occurs for an impact energy of about 30 J, whereas such a critical energy increases to about 35 J (about +17%) for the more thick and weight CFRP laminate. Also, the maximum force of the thicker CFRP laminate is higher than that of the hybrid C-KFRP (about +10%).

In order to compare the two laminates having different thickness and specific weight the relieved impact forces have been divided to the corresponding actual thickness and specific weight obtaining the specific $F_i(s)^*$ curves shown in Figure 2.

[Figure 6 near here]

From Figure 2a it is possible to observe how the hybridization lead to an increment of the specific energy to complete penetration of about +15% (from 10.6 to 11.7 kJmm²/g) and a slight superior increment of the maximum force of about 18%.

From Figure 2b it is seen instead how for an impact energy of 30 J (maximum energy supported by the hybrid composite) the hybrid composite exhibits an increment of the specific energy of about 34% (from 8.75 to 11.75 kJmm²/g)

In addition, in order to corroborate that the impact strength increases if the hybrid lamina coincide with the superficial one subjected to the impact, the relationship between impacting surface (the hybrid one or the opposite one reinforced only by carbon fibers) the two different impact tests have been performed on the hybrid composite by varying the face exposed to the impactor. Specifically, the sample called C-KFRP(c) has been positioned with the ± 45 twill carbon lamina exposed to direct contact with the impactor. As an example, the impact curves for the impact energy level of 30 J are reported in the following Figure 3 that clearly shows how the peak value of the force increases of about +25%. Also, the application of the impact load on the hybrid face permits to maximize the hybridization effects with a significant increase of about +60% of the energy $E_{a,e}$ absorbed during the elastic phase (without any residual damage of the material). As expected, negligible is indeed the differences in term of

total energy absorption, being the material the same in the two different loading conditions.

[Figure 7 near here]

In Table 2 the main specific impact parameters as peak force F_i^{MAX*} , E_a^* and $E_{a,e}^*$ are reported.

[Table 3 near here]

From Table 2 it is corroborated how at a fixed impact energy level, the peak force decreases by passing from CFRP to the C-KFRP, whereas the total absorbed energy increases from about +47% to about 34% moving from 20 J to 30 J. Considering instead the condition of complete penetration the specific total energy absorbed by the hybrid composite is higher than that of the basic CFRP of about +11% whereas the specific elastic absorbed energy increases of about +43% (from 3000 to 4285 J mm² g⁻¹). In other word, the hybrid laminate has a higher capacity to absorb energy in the elastic field, i.e. without any residual damage of the material, and then of the component subjected to the impact loading.

Plotting the values of specific energy absorbed, shown in Table 2, by means of a bar graph (see

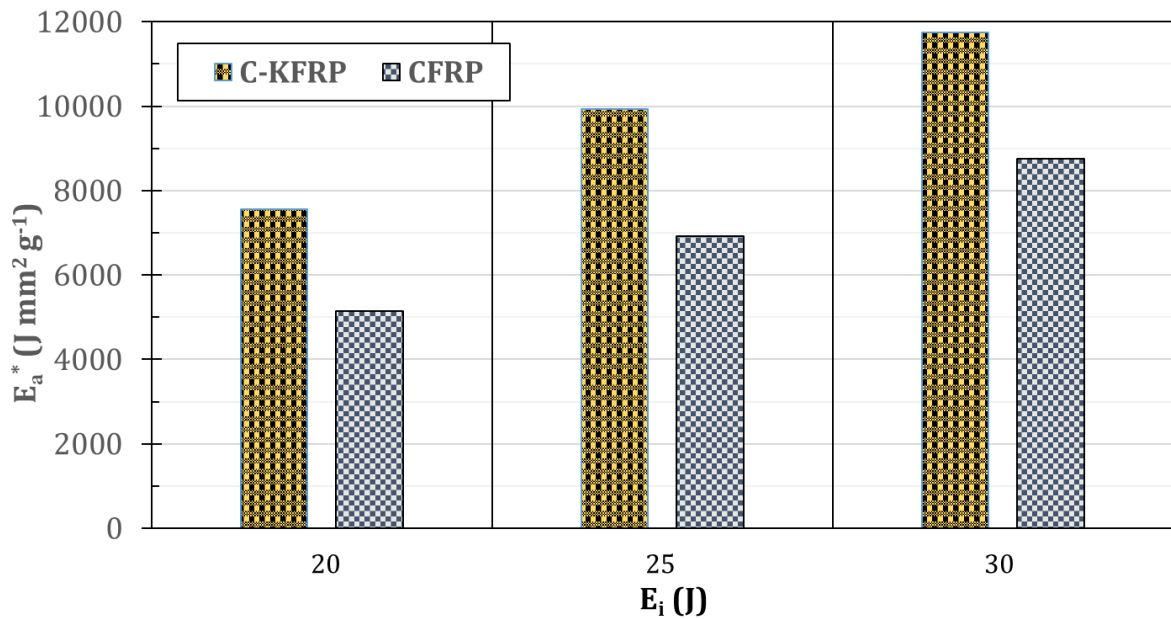


Figure 4), it is more easy to notice how for a fixed impact energy the specific energy absorbed by the C-KFRP is always appreciably superior to that absorbed by the CFRP with increment that vary from about 40% to about 30% when the impact energy pass from 20 to 30 J.

[Figure 8 near here]

Finally, in terms of specific strength, it can be said that hybridization of only the surface lamina on a CFRP composite laminate consisting of 3 laminae, leads to substantial benefits.

3.3 *Non-destructive assessment of impact damage.*

From the visual inspection of the specimens after the impact tests, the progressive increasing damage can be highlighted as the impact energy reaches complete perforation. Figure 5 shows the damaged surfaces, both front and back sides,

that occurs in both laminates subjected to impact loading with impact energy level that leads to complete penetration (30 J and 35 J for C-KFRP and CFRP, respectively). The front side shown in figure was exposed to the contact with the striker during the impact event.

[Figure 9 near here]

Analyzing the front view of each damaged surface shown in Figure 5, the circular imprint left by the striker can be easily detected. The back surfaces show instead different types of damage, based also on the face exposed to the impact. In more detail, the C-KFRP(c) hybrid composite impacted on the carbon side shows a larger damaged area characterized by diamond-shaped fracture in the back face. Hybrid laminate C-KFRP(c) if compared to the C-KFRP laminate impacted on the hybrid side, it shows a circular fracture made of several radial cracks with delaminations mixed with fibers breakage. From such mechanical response it can be deduced how the damage to the surface in the lower face of the specimen is influenced by the type of lamina which is subjected to the impact event.

A deeper visual inspection of the mechanical damage in hybrid laminates subjected to impact energy far from perforation, highlights that the damage is different if the impact occurs from the side of the hybrid lamina rather than from the side of carbon one. As an example, the optical microscopies at a magnification of 7.5X of the impacted area for an energy of 15 J are shown in Figure 6a and b. As expected, the extent of the impact damage is more limited for the hybrid side and the damage involves both kevlar and carbon fibers. There is a tensile failure along the two orthogonal directions. For the specimen subjected to impact from the side of the carbon lamina,

being the is latter at an orientation of $\pm 45^\circ$, the damage follows the direction of the fibers, with breaking due to tensile load (Figure 6b).

For energies close to total perforation (25 J), the detected damage consists in significant fracture due to tensile load in the 0/90 directions for aramidic fibers (Figure 6c); the carbon fibers are instead mainly subjected to intra-laminar failure in the direction parallel to the fiber itself (Figure 6d). The carbon lamina has the same modalities detected for impact energy equal to 15 J, with evident fracture of the matrix (the images were acquired with a polarizing lens to highlight the fractured parts of the matrix). Furthermore, the fracture of the fibers appears very brittle (with clear interruption of the single filaments) for the carbon fibers, if compared to the aramid ones, which shows mechanical damage distributed in a wider area.

[Figure 10 near here]

The NDE allowed a quantification of the impact effects through the measurement of the extension of the damaged area and the assessment of the actual failure modes.

In Figure 7, 3D reconstruction by CT, PAUT C-scans and PT thermograms are reported for impact damaged C-KFRP specimens at 15 J (a), impact damaged C-KFRP specimens at 20 J (b), impact damaged C-KFRP specimens at 25 J (c), impact damaged C-KFRP(c) specimens at 15 J (d) and impact damaged C-KFRP(c) specimens at 25 J (e). As above mentioned, the specimens identified as C-KFRP(c) were subjected to impact test on the side of carbon lamina, which is the lamina on the opposite side for C-KFRP specimens. All the images are referred to the side in which the impact event occurred (front view).

[Figure 11 near here]

Analyzing the results obtained by the different techniques, for the specimens subjected to increasing impact energy (15, 20 and 25 J) from the side of the carbon/kevlar hybrid lamina, it is evident that the damage revealed through such techniques is more extensive than that observed by visual analysis. This is a typical behavior of laminates, which require volumetric inspection techniques to quantify the damage due to impact loading in a reliable way. The extension of the damaged area increases as the impact energy increases (Figure 7a, b and c) and the damage entity becomes more severe.

Regarding the specimens that were exceptionally subjected to the impact on the side of the carbon lamina (Figure 7d and e), the damaged area has a diamond shape, with the faces parallel to the orientation of the fibers at $\pm 45^\circ$, which are firstly involved in the impact damage mechanisms (as reported in **Errore. L'origine riferimento non è stata trovata.**). Thus, the damaged area is strictly dependent on the arrangement of the fibers lying on the face where the impact occurs.

Even though, at the same impact energy, the diameter of the damage can have similar values, the extension of the damage is greater for the specimen that has been subjected to the impact on the side of the carbon lamina, which gives rise to a cross-shaped fracture mode. Such behavior is due to the inability of carbon layer to withstand flexural strains, as its bending modulus is slightly higher than hybrid lamina one (Table 1). It is important to observe how all the considered non-destructive techniques supported the above reported considerations. However, the PAUT-C Scan seems the technique that shows the better sensitivity giving more detailed damage maps.

For a more accurate in-depth damage analysis, in Figure 8 the tomograms of the middle section and the corresponding S-scan for the C-KFRP specimens (hybrid lamina on the side of the impact event) tested at 15 J (a), 20 J (b) and 25 J (c) are reported. In Figure 8 (d) and (e) shown instead both tomograms and S-scans of the C-KFRP(c) specimens (impacted on the side of carbon lamina) at 15 J (d) and 25 J (e).

[Figure 12 near here]

From the analysis of the tomograms and S-scans, shown in Figure 8 and referred to the section at the maximum indentation depth, it is evident that the internal damage mechanisms are common for the two types of load configuration: extensive delaminations are detected, whose extension grows as the impact energy increases, as well as fracture of the laminae and of the matrix. Significant interlaminar fractures in the specimens subjected to impact from the side of the carbon lamina appears to be present both at 15 J and at 25 J. The same behavior is also observed for the specimens correctly impacted on the hybrid side, with the difference that in this case the contribution of the hybrid lamina is more evident and the internal damage have an appreciable minor extension along to the section axis. This behavior is evidenced also by the higher out of plane displacement of the specimens. The study of the collapse mode highlights that the fracture of both matrix and fiber - mainly the aramid one - contributes significantly to the energy absorption. Indeed, by analyzing the results of the impact tests shown in Figure 1b, the significant load dropping that occurs at about 4 mm in depth for non-perforated specimens, can be attributed to the damage shown by the CT reconstructions and C-scans (blue color) shown in Figure 7. Considering that such damage is concentrated in some parts of the impacted area, the sections in Figure 8

confirm that it is due to the large delaminations experienced by the damaged specimens (highlighted by blue ellipse).

In Figure 9, DR images, PAUT C-scans and PT thermograms are shown for impact damaged CFRP specimens at 20 J (a), at 25 J (b), at 30 J (c) and at 35 J (d). All the images are referred to the front view of the specimens, which is the face subjected to the impact test in the actual service loading.

The comparison between of the DR images with that obtained by the CT for the CFRP laminate shows how DR have lower sensitivity to the surface damage. Better sensitivity is instead shown by the PAUT-C scan: the shape of the damaged area of CFRP laminate is similar to C-KFRP one. This behavior is mainly due to the same stacking sequence. In particular, C-scans reveal that the damage is equally distributed in the perimeter of the damaged area. Such behavior can explain the rapid load loss, after the peak, shown in the impact curves in Figure 1b and d. Intermediate results have produced by the PT thermograms.

[Figure 13 near here]

In Figure 10, PAUT S-scans of the CFRP specimens are shown and are referred to the section of the specimens where higher indentation depth and out-of-plan displacement were evaluated. Thus, the global residual deformation of the specimen due to bending can be evaluated. Carbon fiber laminates have higher stiffness, which leads to more severe damage due to shear occurring during the impact event. On the other side, higher modulus allows CFRP laminates to withstand high stresses, but the impact event has a lower time duration (Figure 1a and c) if compared to C-KFRP laminates. The results of such behavior of CFRP specimens deal to smaller extension of the

damaged area, to deeper indentation and less displacement than C-KFRP ones. Such results are consistent with literature [38].

[Figure 14 near here]

As shown in visual inspection analyses (Figure 5), the low velocity impact event in CFRP laminates causes a barely visible damage, which can be easily detected by all the non-destructive techniques proposed in this research. Nevertheless, only PAUT was capable to reveal that the detected delaminations were sub-superficial (Figure 10) and were mainly due to the very limited out-of-plane displacements ability of carbon laminae, if compared to the K-CFRP specimens (Figure 8).

Figure 11 shows the measurements of the damage extension in the impacted laminates by using the different techniques. If CT (Figure 11a, C-KFRP laminates) can be considered the most reliable technique (considered as reference one), it can be assessed that flash thermography slightly underestimates the damage; whereas ultrasonic phased array gives a slight overestimation. Considering that the estimation difference among the techniques is not considerable, for this kind of specimens, the reliability of the different techniques is in general very high. Anyway, the practical application of PAUT was more difficult respect to other techniques, due to the high deformation of the specimens, which causes a not perfect contact with the probe (see Figure 7b). The damage extension is fitted by exponential laws (Figure 11a, C-KFRP laminates), which could be useful to estimate the damage length in case of impact in working conditions or in the design phase.

Considering again the C-KFRP specimens, the results are very different if are referred to the impact event of the side on the carbon lamina (Figure 11b, labelled as C-

KFRP(c)). CT has highlighted severe delaminations at early impact energy (15 J), due to the intrinsic stiff behavior of the carbon lamina. Even though the data are limited, if they are compared to that evaluated in the hybrid lamina, the measurements in Figure 11b can be a useful tool to have an idea of the mechanical performance if this kind of laminate is put in working conditions on the wrong side. In Figure 11c, the damage extension measured with DR at 20 J of impact energy is reported but not considered in data interpolation because clearly unreliable.

For what concerns CFRP specimens (Figure 11c), the x-ray technique used to measure the extension of the damage was digital radiography, which is obviously easier to use with a portable equipment if on-site inspections are required to estimate impact damage. The results can be compared to the CT ones, as the latter are presented in the form of sum along x-rays (Figure 7); even though is worthy of mentioning that the focal spot size of the tube is 400 μm (for CT was 250 μm). As a consequence, low damage cannot be correctly detected with this technique, due to an underestimation of the impact damage of about 1/3 respect to PAUT results. The measurements become reliable approaching an impact energy of 25 J and more. Thus, DR technique gives a smaller estimation of the damage, if compared to PT and PAUT, which gives the highest values. Such findings can be explained as follows: in CFRP specimens the most frequent damage mechanism is referred to extensive sub-surface delamination, which DR is not capable to reveal in one shot. In this paper, CT results derive by the superimposition of 1444 projections (can be considered 1444 radiographs) which obviously can catch all the damage mechanisms occurred in each section of the specimens. The trend – and the exponential laws – referred to PAUT and PT are very similar. Thus, it can be assessed that the higher values of damage length measured by

PAUT become more evident for higher impact energies, which cause a deeper damage, difficult to detect with thermal techniques.

[Figure 15 near here]

A direct comparison among the three different approaches (RX methods, PAUT, PT) techniques is reported in Figure 12, whose results are referred to the extension of damage in the specimens impacted at 25 J. It is seen how PAUT gives always higher values of damage extension, due to the high sensitivity of this technique, which can be considered the most appropriate for this kind of materials. The lower sensitivity of pulsed thermography technique, mainly if the damage is very deep, puts in evidence that the underestimation can become remarkable. On the other side, it is worth mentioning that pulsed thermography is very fast, contactless, applicable also for complex geometries and can be considered very useful for giving an immediate idea if impact damage occurred. Digital radiography can be used coupled to another technique, used for confirm damage estimation, and computed tomography can be considered the best technique for this type of material, mainly if the equipment has an adequate focal spot size. Obviously, is not possible to apply such technique for on-site inspections, and its principal use is for laboratory / R&D applications. Thus, PAUT is the best compromise between reliability and time required to obtain quite accurate quantitative results for the hybrid composite considered in the present study.

[Figure 16 near here]

4. Conclusions

The experimental investigation carried out in this research dealt with the evaluation of the aramid hybridization effects in CFRP, usually used for manufacturing parts of racing cars subjected on impact events (ailerons, bumpers, etc.). Static tensile and bending tests, as well as low velocity impact tests and non-destructive evaluation of the impact damage were performed in order to assess the effect of hybridization on the actual mechanical performance and on the damage extension.

Although hybridization lead to a decrease of the tensile strength of about -30%, along with a reduction of the tensile modulus of about -15%, it leads to a significant increases of the failure energy in both static bending (+25%) and low-velocity impact loading (+43%) by considering the specific elastic absorbed energy.

Considering the NDE of the damage related to impact loading, the results obtained by application CT, PAUT, PT and DR techniques, have shown that PAUT gives a slight overestimation of the damage, but considering that is the best compromise among sensitivity, time required to obtain reliable results, applicability on composites and safety issues, it can be considered the most appropriate technique to evaluate impact damage. It can be surely used in common with other techniques, such as pulsed thermography, which is very fast and easy to perform, and gives reliable results for thin composites (generally, it gives a slight underestimation of the damage).

Among x-rays techniques, without any doubt the most appropriate technique for this kind of specimens and mechanical damage is CT, but its application is limited to small component or in that cases in which costs aren't important. DR has revealed to give appreciable underestimation of the damage, mainly for low impact energies. Its applicability can be suggested if coupled to other technique and in the cases in which safety issues related to the use x-rays are also taken into account.

Declaration of interest statement

The authors report there are no competing interests to declare.

References

- [1] Das S. The Cost of Automotive Polymer Composites: a Review and Assessment of DoE's Lightweight Materials Composites Research. Oak Ridge Natl Lab 2001. <https://doi.org/10.2172/777656>.
- [2] Flynn J, Amiri A, Ulven C. Hybridized carbon and flax fiber composites for tailored performance. *Mater Des* 2016;102:21–9. <https://doi.org/10.1016/j.matdes.2016.03.164>.
- [3] Kureemun U, Ravandi M, Tran LQN, Teo WS, Tay TE, Lee HP. Effects of hybridization and hybrid fibre dispersion on the mechanical properties of woven flax-carbon epoxy at low carbon fibre volume fractions. *Compos Part B Eng* 2018;134:28–38. <https://doi.org/10.1016/j.compositesb.2017.09.035>.
- [4] Naveen J, Jawaid M, Zainudin ES, Sultan MTH, Yahaya R. Mechanical and moisture diffusion behaviour of hybrid Kevlar/Cocos nucifera sheath reinforced epoxy composites. *J Mater Res Technol* 2019;8:1308–18. <https://doi.org/10.1016/j.jmrt.2018.07.023>.
- [5] Yang Z, Liu J, Wang F, Li S, Feng X. Effect of fiber hybridization on mechanical performances and impact behaviors of basalt fiber/UHMWPE fiber reinforced epoxy composites. *Compos Struct* 2019;229:111434. <https://doi.org/10.1016/j.compstruct.2019.111434>.
- [6] Bandaru AK, Patel S, Sachan Y, Ahmad S, Alagirusamy R, Bhatnagar N. Mechanical behavior of Kevlar/basalt reinforced polypropylene composites. *Compos Part A Appl Sci Manuf* 2016;90:642–52. <https://doi.org/10.1016/j.compositesa.2016.08.031>.
- [7] Yahaya R, Sapuan SM, Jawaid M, Leman Z, Zainudin ES. Effect of layering sequence and chemical treatment on the mechanical properties of woven kenaf-aramid hybrid laminated composites. *Mater Des* 2015;67:173–9. <https://doi.org/10.1016/j.matdes.2014.11.024>.
- [8] Feng NL, Malingam SD, Jenal R, Mustafa Z, Subramonian S. A review of the tensile and fatigue responses of cellulosic fibre-reinforced polymer composites, *Mech Adv Mater Struct* 2020;27:8, 645-660, DOI: 10.1080/15376494.2018.1489086
- [9] Chen Q, Zhao Y, Zhou Z, Rahman A, Wu X, Wu W, et al. Fabrication and mechanical properties of hybrid multi-scale epoxy composites reinforced with conventional carbon fiber fabrics surface-

- attached with electrospun carbon nanofiber mats. *Compos Part B* 2013;44:1–7.
<https://doi.org/10.1016/j.compositesb.2012.09.005>.
- [10] Zhang J, Chaisombat K, He S, Wang CH. Hybrid composite laminates reinforced with glass / carbon woven fabrics for lightweight load bearing structures. *Mater Des* 2012;36:75–80.
<https://doi.org/10.1016/j.matdes.2011.11.006>.
- [11] Muñoz R, Martínez V, Sket F, González C, Llorca J. Mechanical behavior and failure micromechanisms of hybrid 3D woven composites in tension. *Compos Part A Appl Sci Manuf* 2014;59:93–104. <https://doi.org/10.1016/j.compositesa.2014.01.003>.
- [12] Batista ACM., Oliverira JF., Aquino EM. Structural Degradation and Mechanical Fracture of Hybrid Fabric Reinforced Composites. *Polym Eng Sci* 2016;56:657–68.
<https://doi.org/10.1002/pen.24292>.
- [13] Batista ACMC, Tinô SRL, Fontes RS, Nóbrega SHS, Aquino EMF. Anisotropy and holes in epoxy composite reinforced by carbon/glass and carbon/aramid hybrid fabrics: Experimental and analytical results. *Compos Part B Eng* 2017;125:9–18.
<https://doi.org/10.1016/j.compositesb.2017.05.066>.
- [14] Biswas D, Ray C. Effect of hybridisation in laminated composites on the first ply failure behaviour: Experimental and numerical studies. *Int J Mech Sci* 2019;161–162.
<https://doi.org/10.1016/j.ijmecsci.2019.105057>.
- [15] Felipe RCTS, Felipe RNB, Batista ACMC, Aquino EMF. Influence of environmental aging in two polymer-reinforced composites using different hybridization methods: Glass/Kevlar fiber hybrid strands and in the weft and warp alternating Kevlar and glass fiber strands. *Compos Part B Eng* 2019;174:106994. <https://doi.org/10.1016/j.compositesb.2019.106994>.
- [16] de Medeiros RJ, da Nóbrega SHS, De Aquino EMF. Failure theories on carbon/Kevlar hybrid fabric based composite laminate: Notch and anisotropy effects. *Mater Res* 2019;22.
<https://doi.org/10.1590/1980-5373-MR-2018-0099>.
- [17] Oliveira JF de S, Leão MA, Batista ACMC, Tinô SRL, de Aquino EMF. Study on Mechanical Properties and Fracture in Epoxy Composites Reinforced by Hybrid Twill Fabrics. *Fibers Polym* 2018;19:1109–18. <https://doi.org/10.1007/s12221-018-7838-3>.
- [18] Valença SL, Griza S, De Oliveira VG, Sussuchi EM, De Cunha FGC. Evaluation of the mechanical behavior of epoxy composite reinforced with Kevlar plain fabric and glass/Kevlar

- hybrid fabric. *Compos Part B Eng* 2015;70:1–8.
<https://doi.org/10.1016/j.compositesb.2014.09.040>.
- [19] Alsaadi M, Erklığ A, Alrawi H. Effect of S-glass fabric on the mechanical characteristics of a hybrid carbon/aramid fabric reinforced epoxy composites. *Mater Res Express* 2017;4.
<https://doi.org/10.1088/2053-1591/aa6bab>.
- [20] Wan YZ, Lian JJ, Huang Y, Wang YL, Chen GC. Two-step surface treatment of 3D braided carbon / Kevlar hybrid fabric and influence on mechanical performance of its composites 2006;429:304–11. <https://doi.org/10.1016/j.msea.2006.05.084>.
- [21] Singh SB, Chawla H, Ranjitha B. Hybrid effect of functionally graded hybrid composites of glass–carbon fibers, *Mech Adv Mater Struct* 2019; 26:14, 1195-1208, DOI: 10.1080/15376494.2018.1432792
- [22] Bulut M, Erklığ A. An experimental investigation on damage characteristics of laminated hybrid composites subjected to low velocity impact. *Polym Compos* 2018;39:3129–39.
<https://doi.org/10.1002/pc.24319>.
- [23] Hosur M V, Adbullah M, Jeelani S. Studies on the low-velocity impact response of woven hybrid composites 2005;67:253–62. <https://doi.org/10.1016/j.compstruct.2004.07.024>.
- [24] Sarasini F, Tirillò J, Ferrante L, Valente M, Valente T, Lampani L, et al. Drop-weight impact behaviour of woven hybrid basalt-carbon/epoxy composites. *Compos Part B Eng* 2014;59:204–20. <https://doi.org/10.1016/j.compositesb.2013.12.006>.
- [25] Hu Y, Liu W, Shi Y. Low-velocity impact damage research on CFRPs with Kevlar-fiber toughening. *Compos Struct* 2019;216:127–41. <https://doi.org/10.1016/j.compstruct.2019.02.051>.
- [26] Caminero MA, García-Moreno I, Rodríguez GP, Chacón JM. Internal damage evaluation of composite structures using phased array ultrasonic technique: Impact damage assessment in CFRP and 3D printed reinforced composites. *Compos Part B Eng* 2019;165:131-42.
<https://doi.org/10.1016/j.compositesb.2018.11.091>
- [27] I. Papa, L. Boccarusso, A. Langella, V. Lopresto. Carbon/glass hybrid composite laminates in vinylester resin: bending and low velocity impact tests. *Compos Struct*, 2020; 232, article 111571.
- [28] Moradi M, Safizadeh MS. Edge disbond detection of carbon/epoxy repair patch on aluminum using thermography. *Compos Sci Technol* 2019;179:41-53.

<https://doi.org/10.1016/j.compscitech.2019.04.031>

- [29] Meola C, Boccardi S, Carlomagno GM, Boffa ND, Monaco E, Ricci F. Nondestructive evaluation of carbon fibre reinforced composites with infrared thermography and ultrasonics. *Compos Struct* 2015;134:845-53. <https://doi.org/10.1016/j.compstruct.2015.08.119>
- [30] Rubio Díaz I, Rodríguez-Millán M, Rusinek M, Miguélez MH, Loya JA. Energy absorption analysis of aramid composite during blunt projectile impact. *Mech Adv Mater Struct* 2021; DOI: 10.1080/15376494.2021.1963020
- [31] Guo R, Xian G, Li C, Huang X, Xin M. Effect of fiber hybridization types on the mechanical properties of carbon/glass fiber reinforced polymer composite rod. *Mech Adv Mater Struct* 2021; DOI: 10.1080/15376494.2021.1974620
- [32] Gaudenzi P, Bernabei M, Dati E, De Angelis G, Marrone M, Lampani L. On the evaluation of impact damage on composite materials by comparing different NDI techniques. *Compos Struct* 2014;118:257-66. <https://doi.org/10.1016/j.compstruct.2014.07.048>
- [33] Epasto G, Distefano F, Gu L, Mozafari H, Linul E. (2020). Design and optimization of Metallic Foam Shell protective device against flying ballast impact damage in railway axles. *Materials & Design*, 196, 109120. <https://doi.org/10.1016/j.matdes.2020.109120>
- [34] Epasto G, Distefano F, Mozafari H, Linul E, Crupi V. Nondestructive Evaluation of Aluminium Foam Panels Subjected to Impact Loading. *Applied Sciences*. 2021; 11(3):1148. <https://doi.org/10.3390/app11031148>
- [35] ASTM D 3039. Standard Test Method for Tensile Properties of Polymer Matrix Composite Materials. 2002.
- [36] ASTM D 7264. Standard Test Method for Flexural Properties of Polymer Matrix Composite Materials.
- [37] ISO 6603-2 00. Plastics - Determination of puncture impact behaviour of rigid plastics. 2000.
- [38] Ying S, Mengyun T, Zhijun R, Baohui S, Li C. An experimental investigation on the low-velocity impact response of carbon–aramid/epoxy hybrid composite laminates. *J Reinf Plast Compos* 2017; 36(6): 422-434. <https://doi.org/10.1177/0731684416680893>

Table 1. Characteristics of the composite laminates considered.

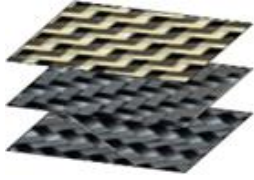
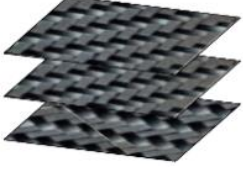
Laminate	Lay-up	V_f [%]	t_L [mm]	ρ [g/cm ³]
C-KFRP	[(0/90)_{c-k}/(0/90)_c/(± 45)_c]	49	1.6	1.54
C-K(t)	Carbon-kevlar pre-preg GA210T (<i>twill</i>) 0/90	45		
C(t)	Carbon pre-preg C630T (<i>twill</i>) 0/90	50		
C(t)	Carbon pre-preg C630T (<i>twill</i>) ± 45	50		
CFRP	[(0/90)_c/(0/90)_c/(± 45)_c]	50	2.0	1.57
C(t)	Carbon pre-preg C630T (<i>twill</i>) 0/90	50		
C(t)	Carbon pre-preg C630T (<i>twill</i>) 0/90	50		
C(t)	Carbon pre-preg C630T (<i>twill</i>) ± 45	50		

Table 1 Flexural properties of the laminates.

Test configuration	Bending strength [MPa]	Bending Modulus [GPa]	Failure Strain [%]	Failure Energy [kJ/m ²]
C-KFRP_(0/90)	485 ± 5.6	21 ± 0.8	4 ± 0.1	14.7
C-KFRP_(±45)	580 ± 9.4	23.5 ± 0.3	2.7 ± 0.6	9.1
CFRP_(0/90)	480 ± 4.4	22.7 ± 0.2	2.1 ± 0.3	5.7
CFRP_(±45)	550 ± 6.7	22.1 ± 0.4	2.4 ± 0.5	4.3

Table 2 Average values of characteristic specific parameters obtained from impact tests.

E_i [J]	<i>Specimen</i>	F_i^{MAX} [kN]	F_i^{MAX*} [kN/(g/mm ²)]	E_a^* [J mm ² g ⁻¹]	$E_{a,e}^*$ [J mm ² g ⁻¹]
20	CFRP	5.35	1857	5150	3478
	C-KFRP	3.98	1694	7557	3246
25	CFRP	5.61	1948	6914	3547
	C-KFRP	4.26	1811	9935	3311
	C-KFRP(c)	3.78	1609	9825	2868
30	CFRP	4.82	1676	8752	2941
	C-KFRP	4.44	1889	11753	4285
	C-KFRP(c)	3.72	1582	11169	2890
35	CFRP	4.93	1713	10624	3004

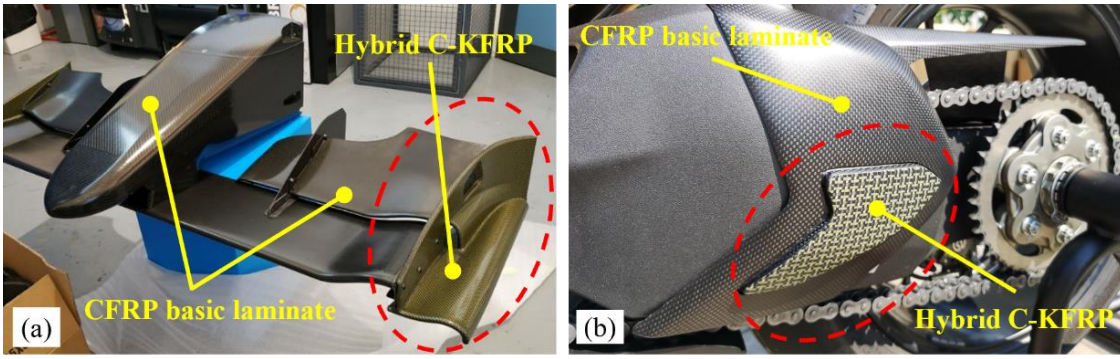


Figure 1

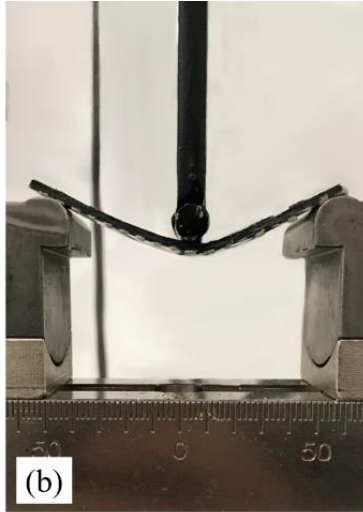


Figure 2

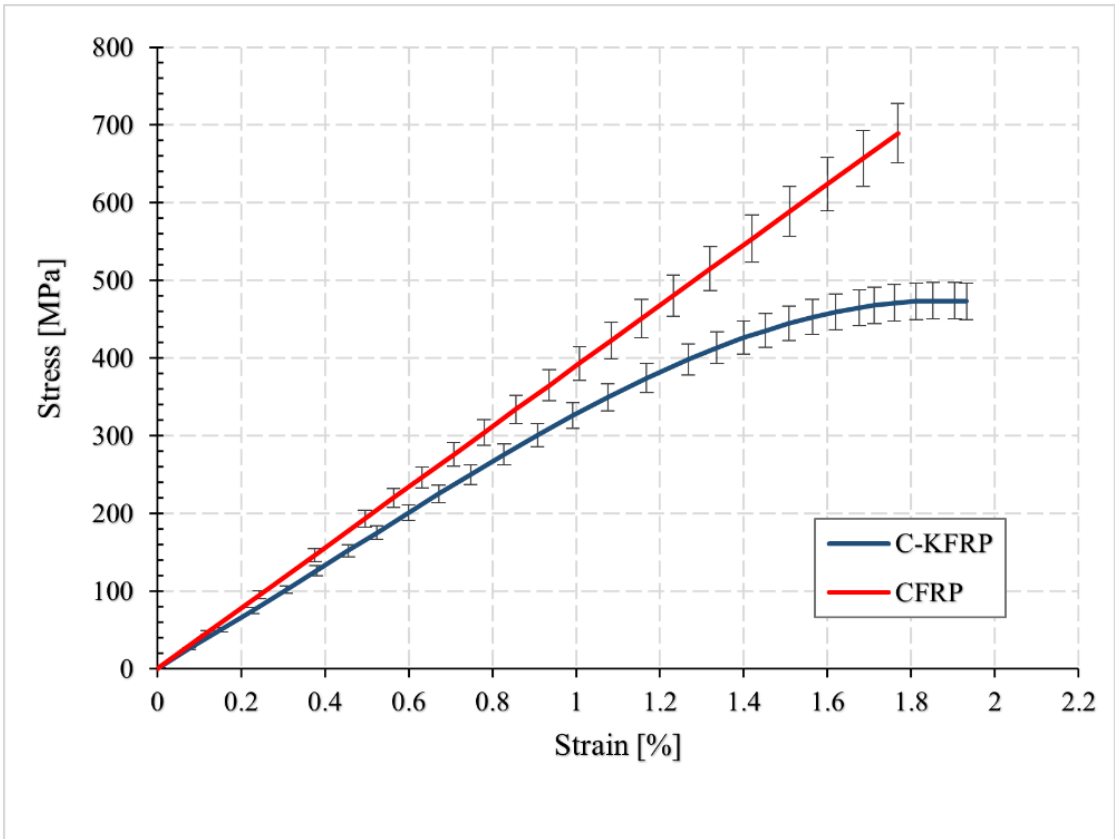


Figure 3

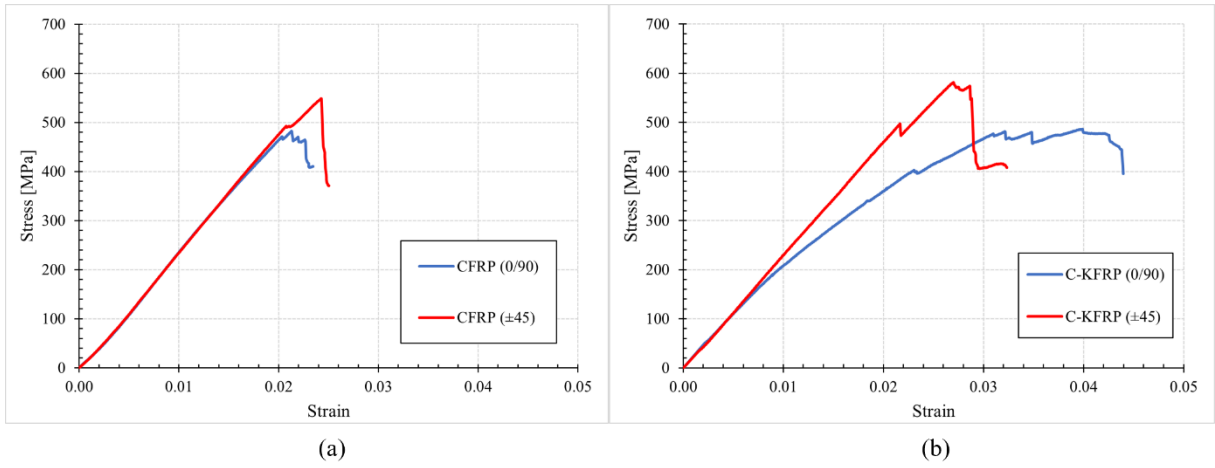
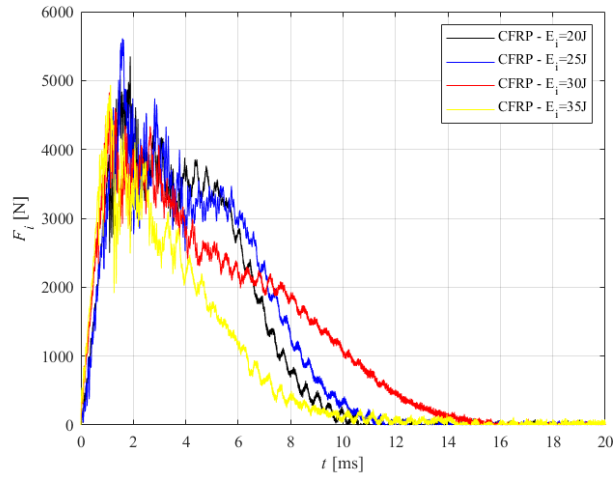
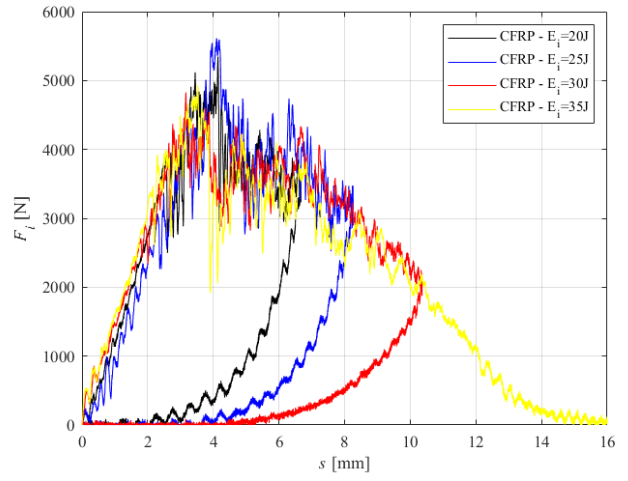


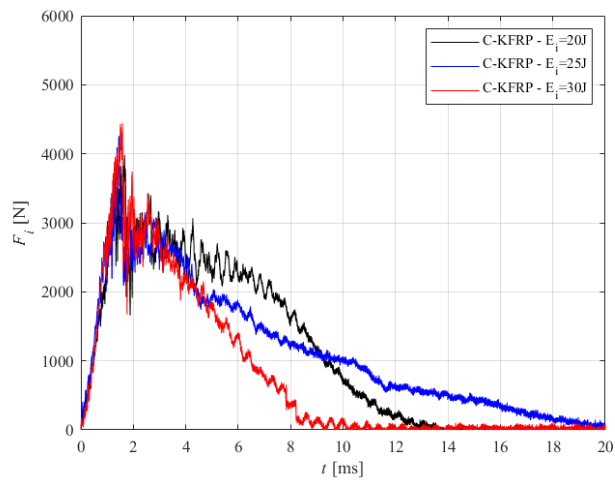
Figure 4



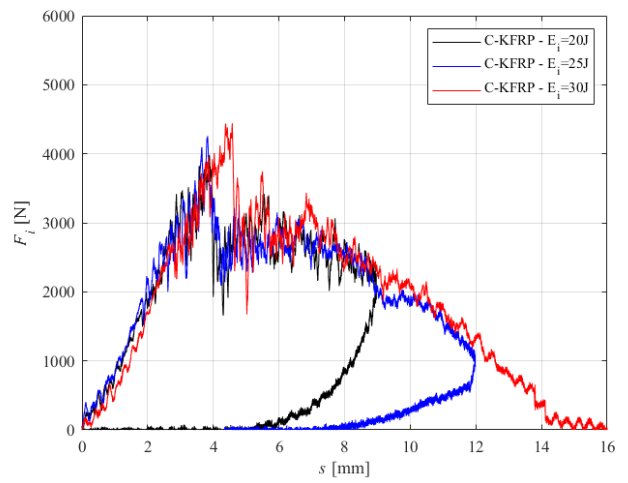
(a)



(b)

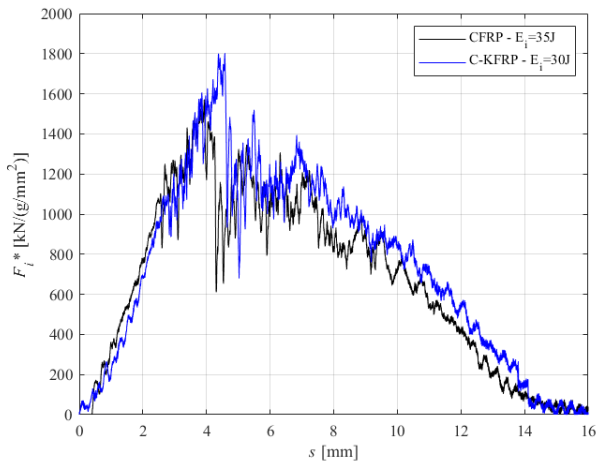


(c)

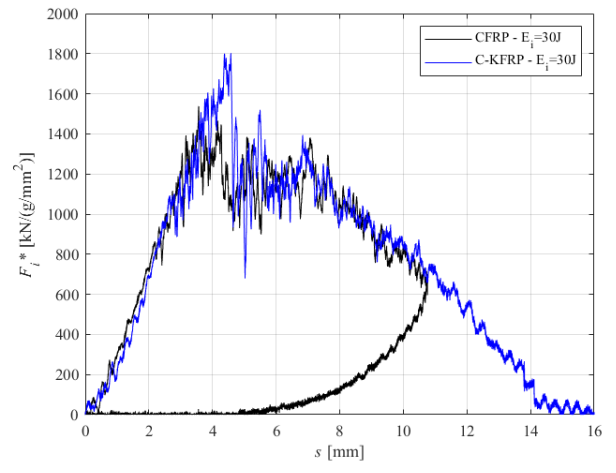


(d)

Figure 1



(a)



(b)

Figure 2

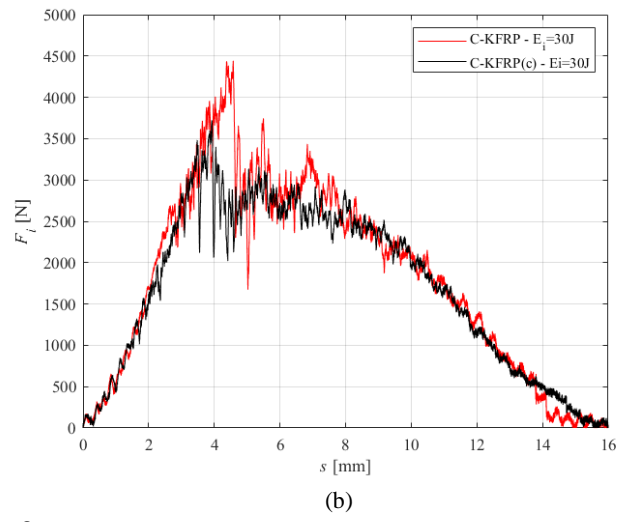
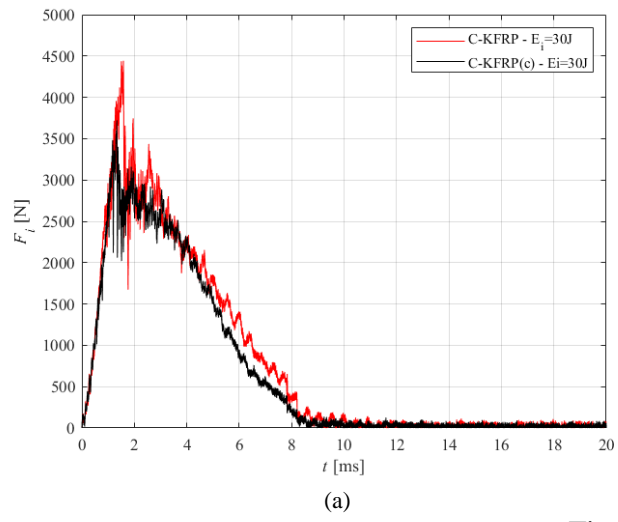


Figure 3

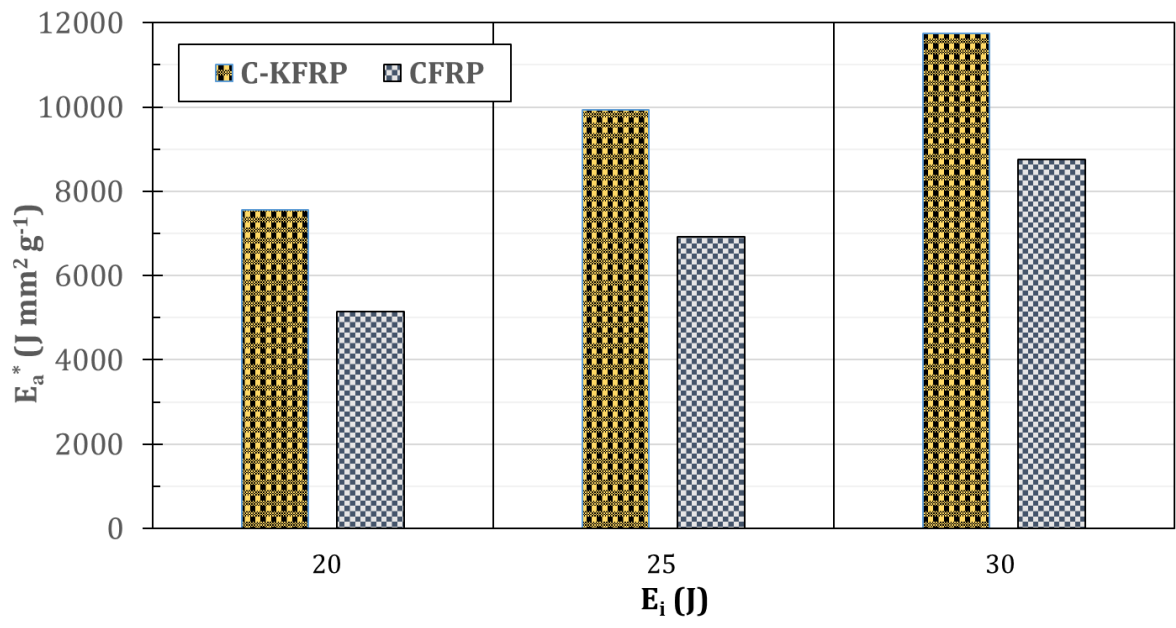


Figure 4

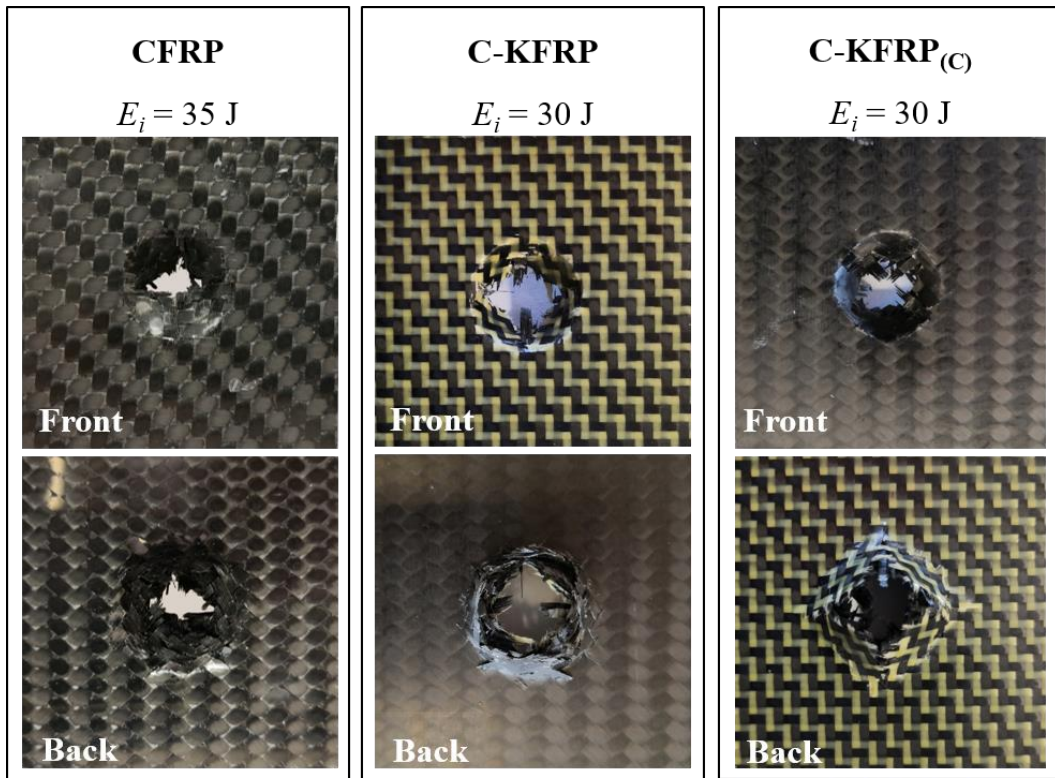
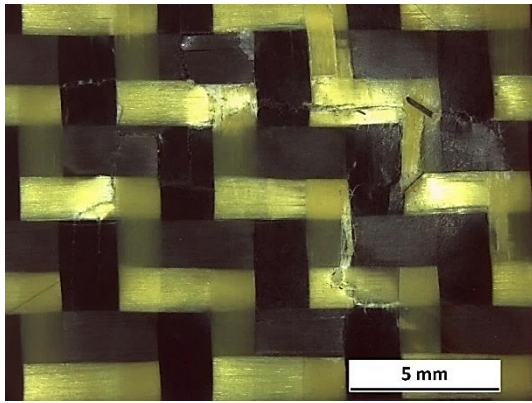
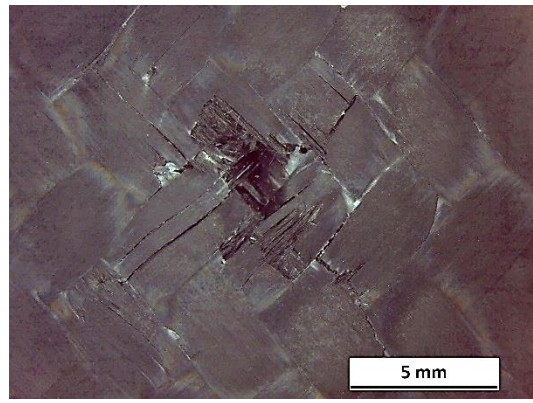


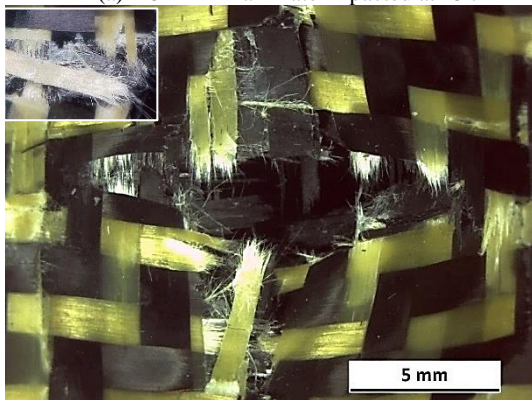
Figure 5



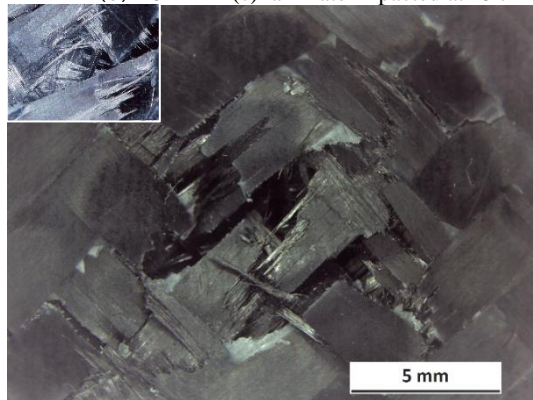
(a) C-KFRP laminate impacted at 15 J



(b) C-KFRP(c) laminate impacted at 15 J



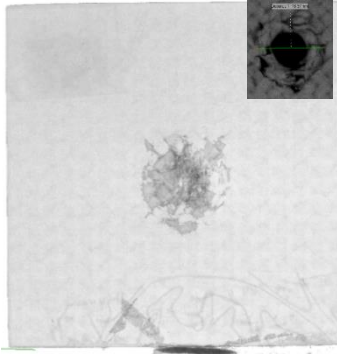
(c) C-KFRP laminate impacted at 25 J



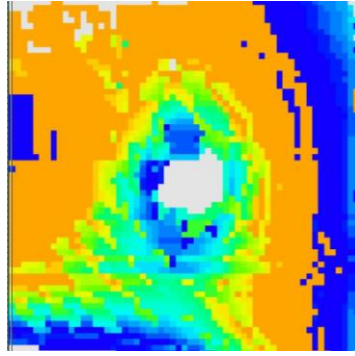
(d) C-KFRP(c) laminate impacted at 25 J

Figure 6

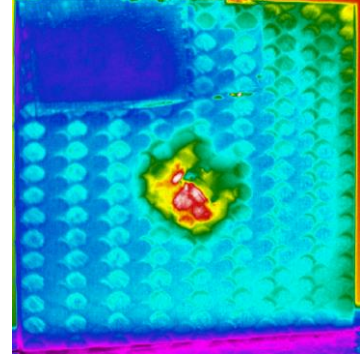
3D CT reconstruction



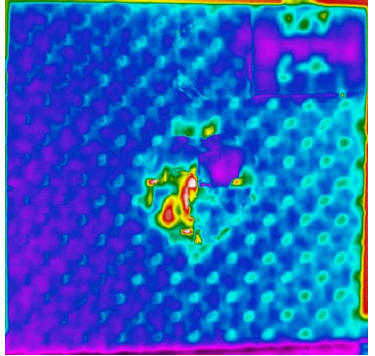
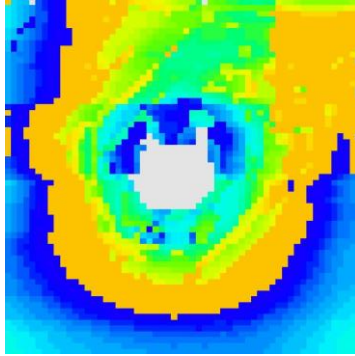
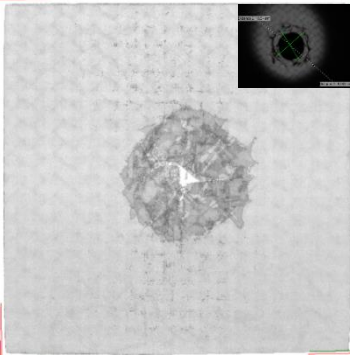
PAUT C-scans



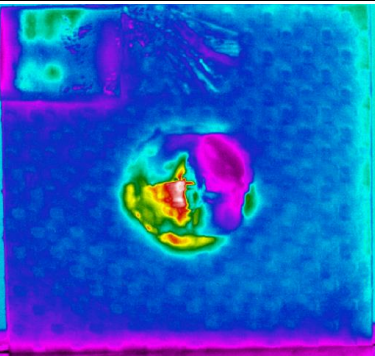
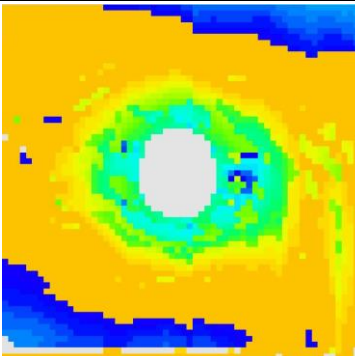
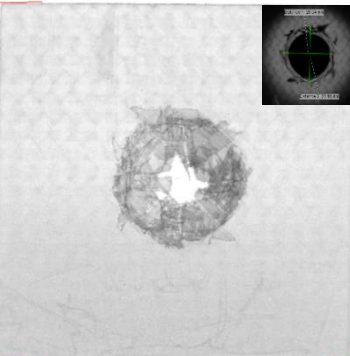
PT thermograms



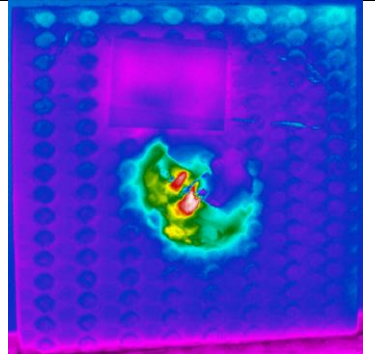
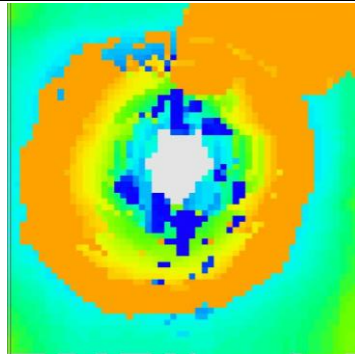
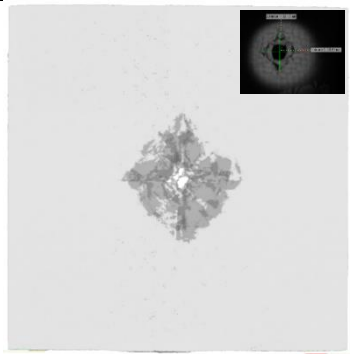
(a) C-KFRP laminate impacted at 15 J



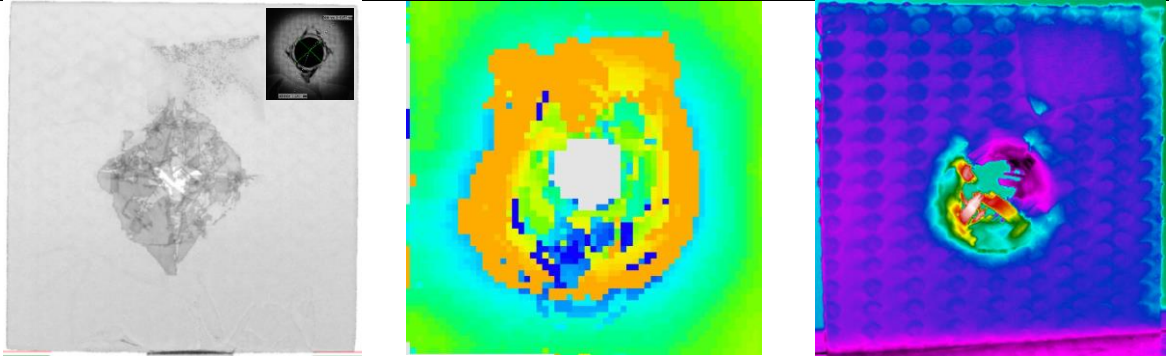
(b) C-KFRP laminate impacted at 20 J



(c) C-KFRP laminate impacted at 25 J

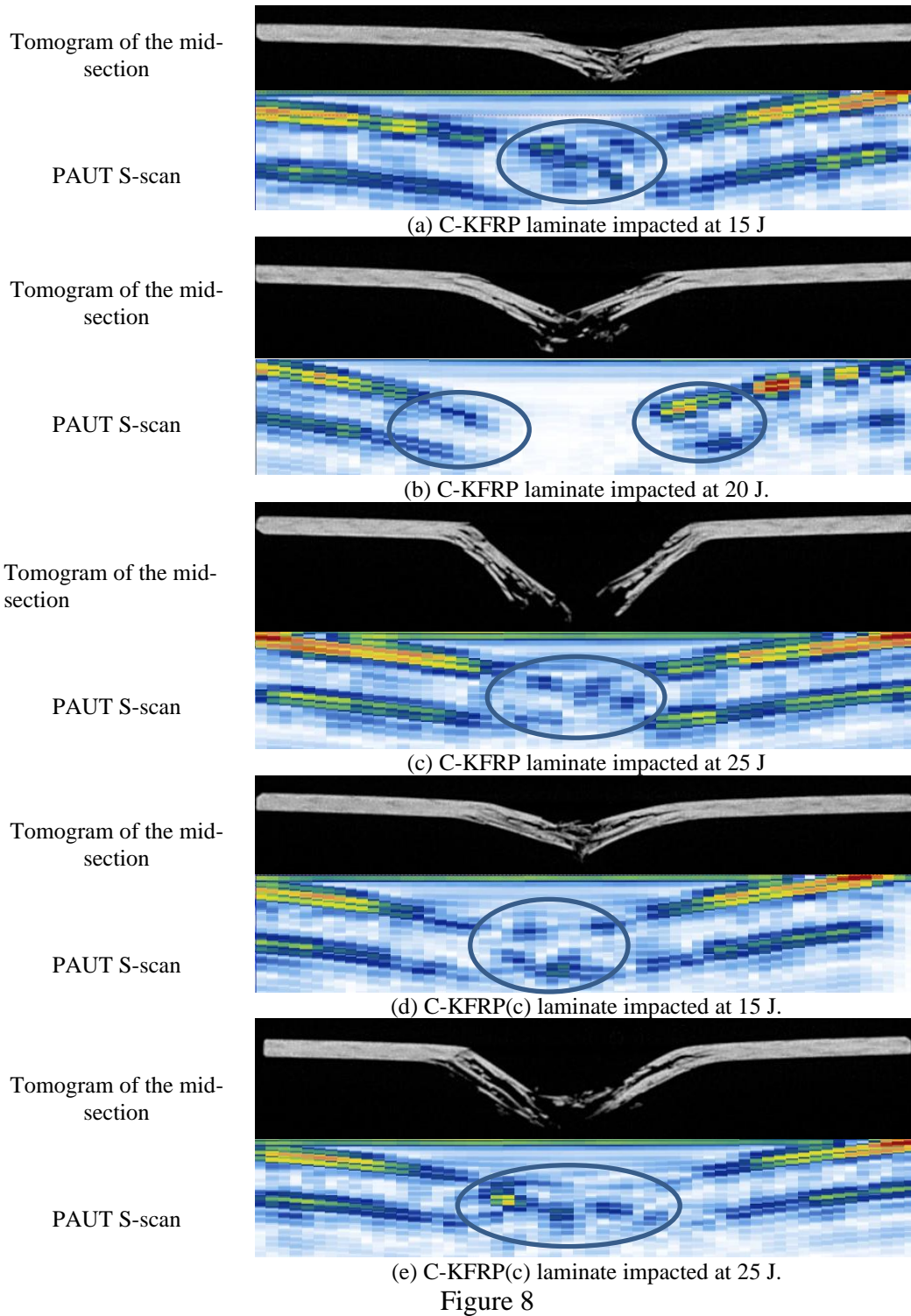


(d) C-KFRP(c) laminate impacted at 15 J



e) C-KFRP(c) laminate impacted at 25 J

Figure 7



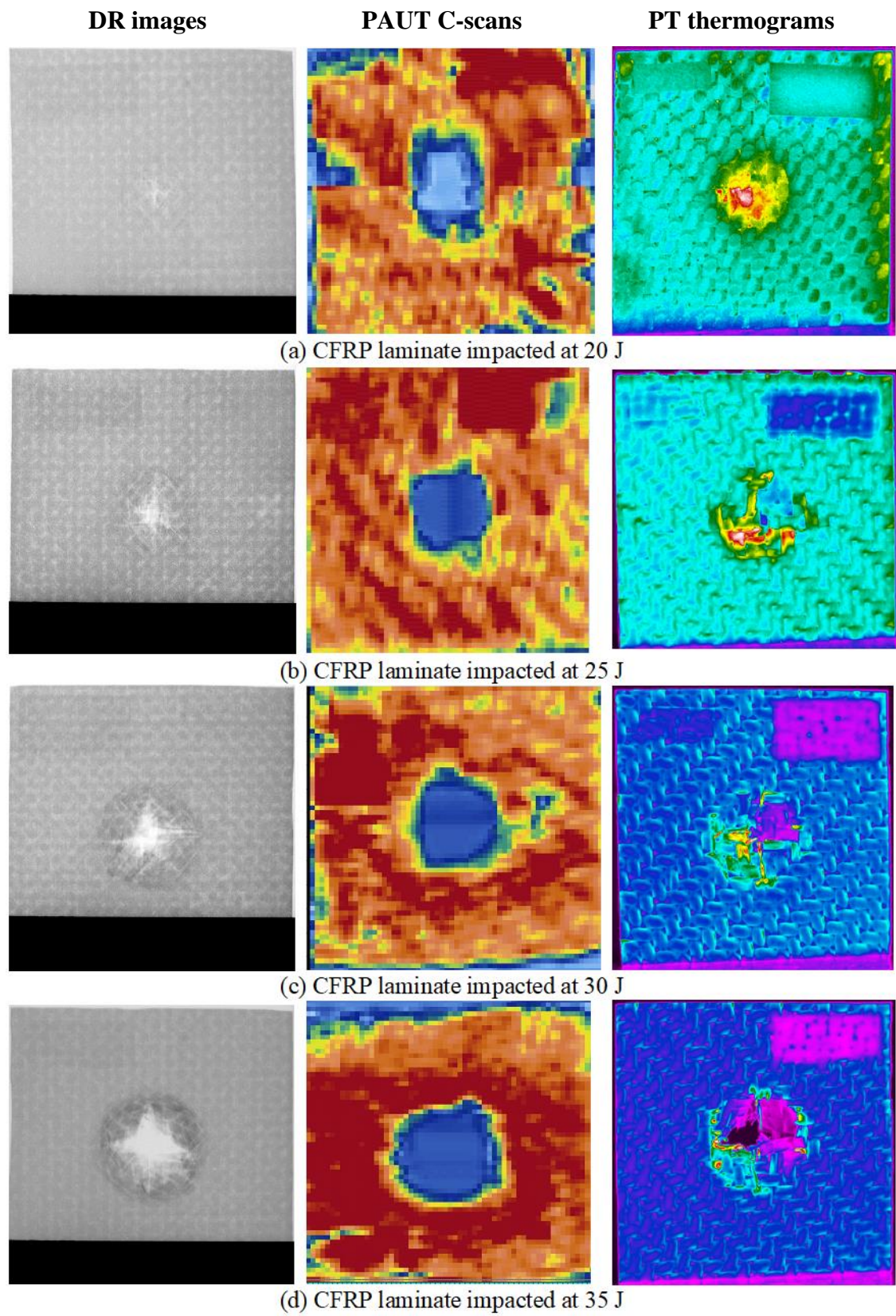


Figure 9

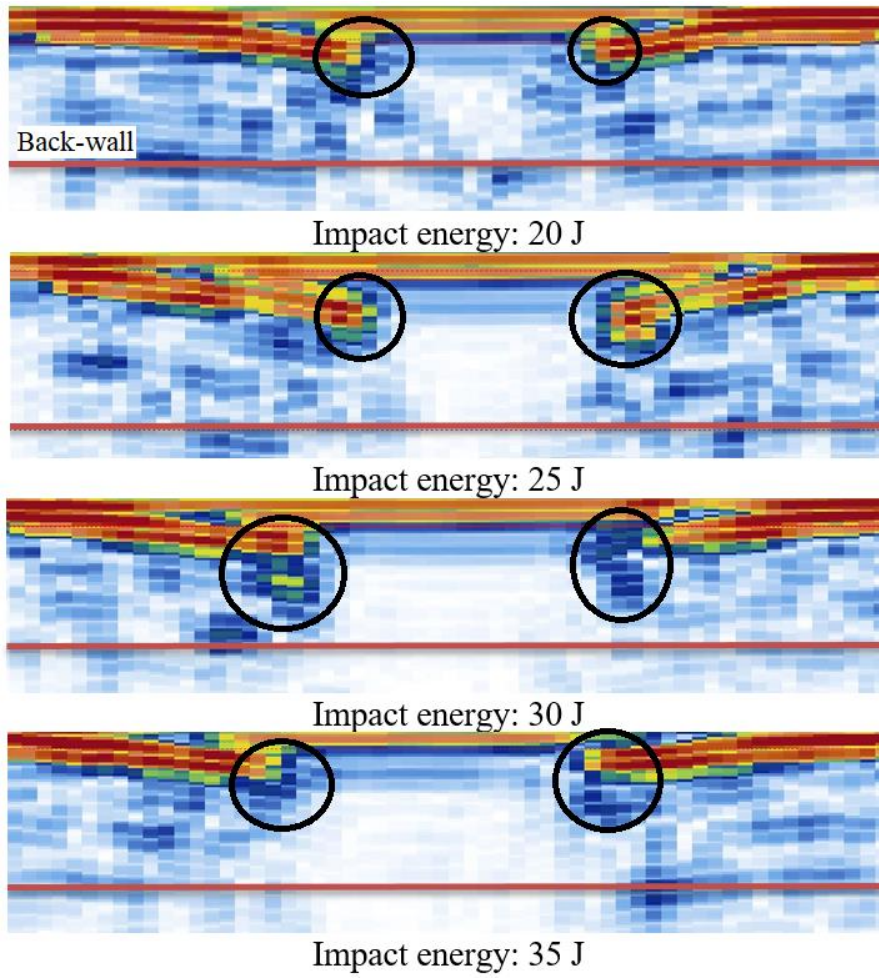


Figure 10

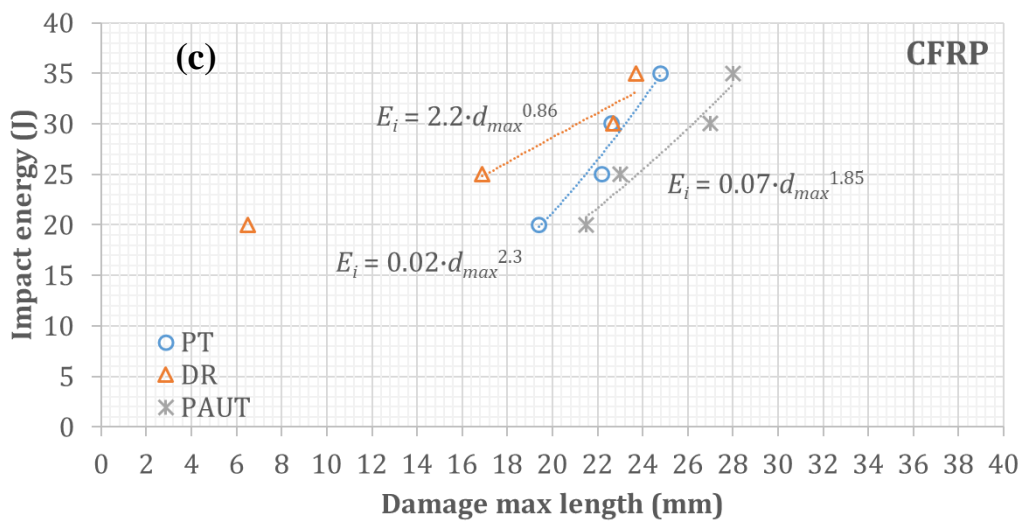
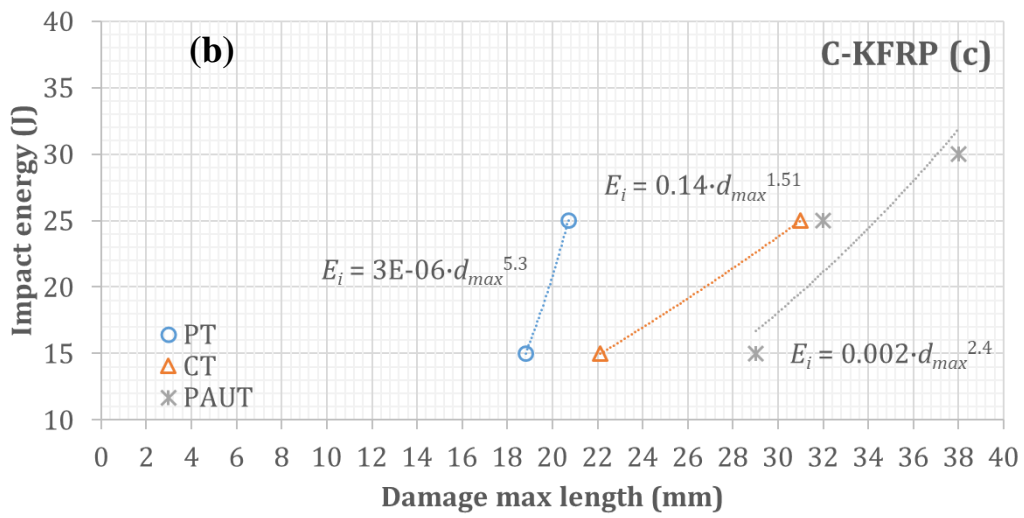
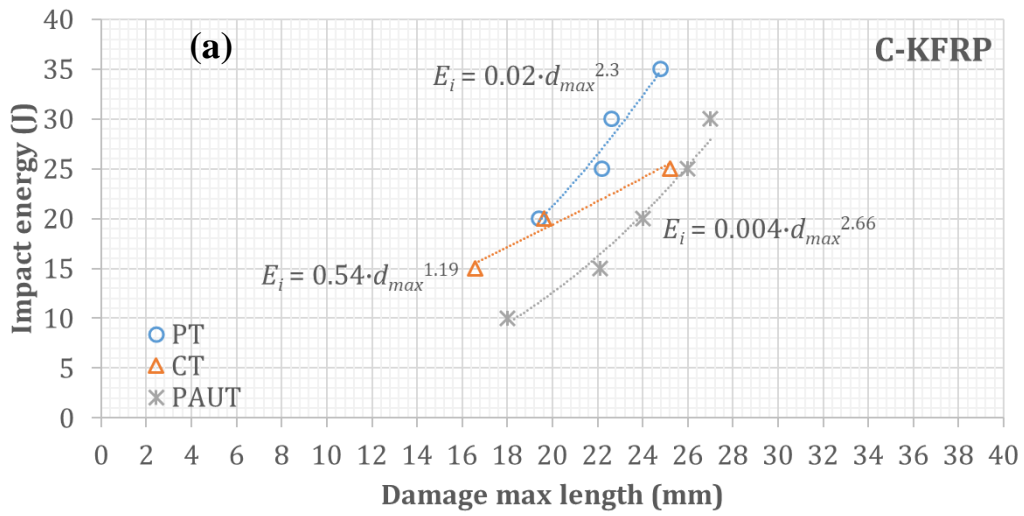


Figure 11

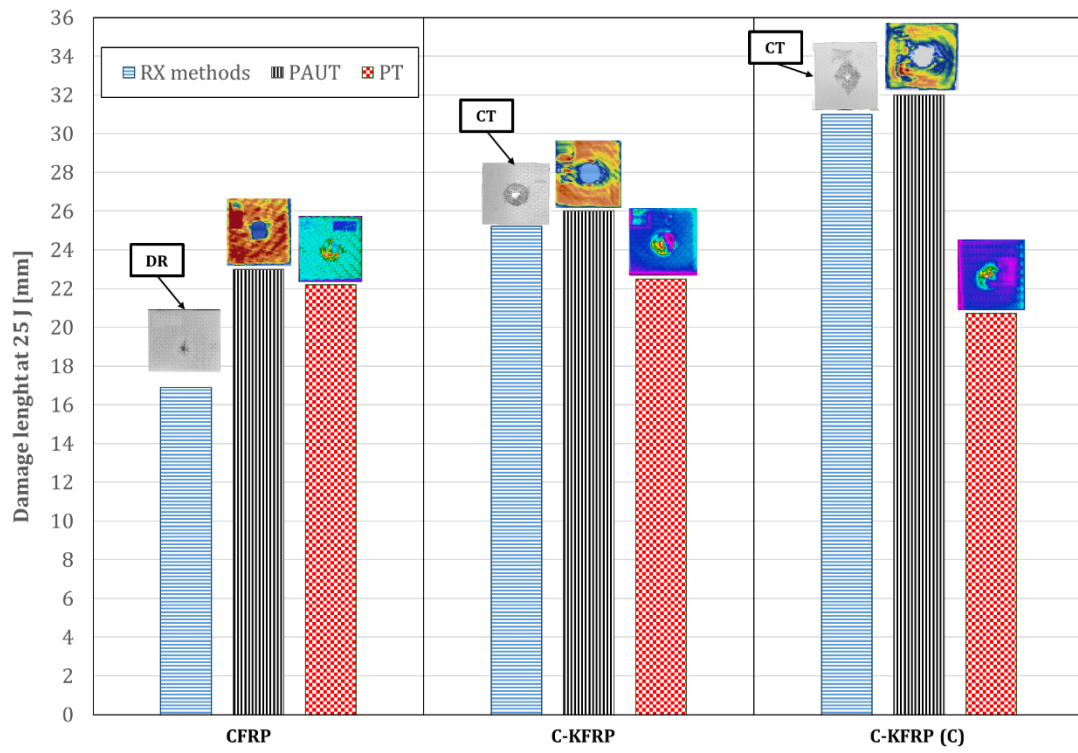


Figure 12

Figure Captions

Figure 1. Example of hybrid laminates type C-KFRP used to increase the impact strength of mechanical components in sport automotive field: (a) aileron ends and (b) lateral bumper.

Figure 13. (a) Static tensile test specimen, (b) static three-point bending test and (c) support system for impact test.

Figure 14. Tensile curves of the two composite laminates examined.

Figure 15. Bending characteristic curves of the (a) C-KFRP and (b) CFRP laminates.

Figure 16. Load-time curve $F_i(t)$ and load-displacement curve $F_i(s)$ relative to composites (a,b) CFRP and (c,d) C-KFRP.

Figure 17. Specific load-displacement curves $F_i(s)^*$ relative to composites CFRP and C-KFRP in the case of (a) complete penetration and in case of (b) impact energy of 30 J.

Figure 18. (a) Load-time curve $F_i(t)$ and (b) load-displacement curve $F_i(s)$ relative to hybrid composite in both configurations with $E_i = 30$ J.

Figure 19. Specific absorbed energy values for the two analyzed composite laminates.

Figure 20. Front and back side of the impacted specimens.

Figure 21. Optical microscopies at 7.5 magnitude for hybrid specimens subjected to impact energy of 15 e 25J: (a) and (c) C-KFRP laminate; (b) and (d) C-KFRP(c) laminate.

Figure 22. Results of NDE for hybrid C-KFRP laminate impacted at different energies.

Figure 23. Tomograms and S-scans of impact damaged specimens at various impact energy levels: (a), (b) and (c), C-KFRP; (d) and (e), C-KFRP(c).

Figure 24. Results of different NDE techniques for CFRP laminate impacted at different energies

Figure 25. PAUT S-scans of the impacted cross-section for the CFRP specimens.

Figure 26 Impact damage extension in the different laminates measured by DR, PAUT and PT.

Figure 27. Comparison among the NDTs for the three different impact events at 25 J in the C-KFRP and CFRP specimens. RX method used for CFRP specimens is DR; for both C-KFRP and C-KFRP(c) is CT.